A Model for Crowd Evacuation Dynamics: 2D Numerical Simulations

Maria Gokieli[1,2(✉)]

[1] Faculty of Mathematics and Natural Sciences - School of Exact Sciences, Cardinal Stefan Wyszyński University, Wóycickiego 1/3, 01-938 Warsaw, Poland
[2] ICM, University of Warsaw, Tyniecka 15/17, 02-630 Warsaw, Poland
m.gokieli@icm.edu.pl

Abstract. In [5] we have proposed a numerical scheme for solving a macroscopic model of crowd dynamics. We apply it here to simulate a room evacuation, for velocity fields derived from the p–Poisson equation. We analyze the stability parameters and the influence of p on the dynamics.

Keywords: Finite elements method · crowd dynamics · advection–diffusion · semi–implicit scheme · CFL condition · p-Laplacian

1 Introduction

In [5] we have considered the following model for pedestrians' movement: if $\Omega \subset \mathbb{R}^2$ is the available environment, $\overrightarrow{V}(x) \in \mathbb{R}^2$ is the velocity of an individual at x, and $\rho(t,x) \in \mathbb{R}$ is the density of the pedestrians at time t and point $x \in \Omega$, the dynamics of ρ is governed by:

$$\partial_t \rho + \operatorname{div}\left(\rho\,\overrightarrow{V}\right) - \kappa\,\Delta\rho = 0 \qquad \text{in } \mathbb{R}^+ \times \Omega\,. \tag{1}$$

This is a regularization ($\kappa > 0$) of the continuity equation proposed originally in this context by Hughes [7,8]

$$\partial_t \rho + \operatorname{div}\left(\rho\,\overrightarrow{V}\right) = 0\,, \qquad \text{in } \mathbb{R}^+ \times \Omega\,. \tag{2}$$

The diffusion term that we add in (1) models a natural random spread of the pedestrians, independently of the direction $\overrightarrow{V}$ they are given.

We consider here that Ω is a room that the pedestrians exit. Consequently, Ω is a bounded domain, the boundary $\partial\Omega$ of Ω is a union of disjoint parts: the walls Γ_w, the exits Γ, and the corners Γ_c. The set of corners is finite; Γ_w and Γ are regular and possess at each point an exterior normal vector $\overrightarrow{\nu}(x)$.

The model requires to be supplied with a velocity field $\overrightarrow{V}$ which defines the evacuation direction. In any nontrivial case it should of course depend on x, and most likely also on $\rho(x)$. This latter dependency appears in the original [7,8] and

R. Wyrzykowski et al. (Eds.): PPAM 2022, LNCS 13827, pp. 343–353, 2023.
https://doi.org/10.1007/978-3-031-30445-3_29

related works, see e.g. [9,13]. It makes however our problem nonlinear. It is also possible to make $\overrightarrow{V}$ depend on other, nonlocal quantities, as the mean value of ρ in some neighborhood of x. We neglect them here – as the nonlocal behaviour is present in our model (1) by the diffusion term. The basic requirement for $\overrightarrow{V}$ so as to get a model of evacuation are the following boundary conditions:

$$\overrightarrow{V} \cdot \overrightarrow{\nu} = 0 \text{ on } \Gamma_w, \tag{3}$$

$$\overrightarrow{V} \cdot \overrightarrow{\nu} > 0 \text{ on } \Gamma. \tag{4}$$

Also, we assume a homogeneous Neumann boundary condition on ρ

$$\nabla\rho \cdot \overrightarrow{\nu} = 0 \quad \text{ on } \Gamma_w \cup \Gamma \tag{5}$$

and the initial condition

$$\rho(0,x) = \rho_0(x) \geq 0. \tag{6}$$

This will ensure the evacuation process (see [5, Lemma 1]).

We are interested here in presenting numerical simulations for the evacuation process, based on (1). We chose a geometry of Ω including obstacles inside the evacuated space and use the numerical scheme of [5]. We have considered there velocity fields $\overrightarrow{V}$ such that

$$\operatorname{div} \overrightarrow{V} \geq 0 \quad \text{ on } \Omega. \tag{7}$$

and have shown that the L^2-norm of the exact solution decreases under the above assumption. The semi–implicit scheme of [5] was shown to be stable and preserving this monotonicity property under a CFL type condition.

We show in the present paper an explicit formula for this CFL condition when (5) is assumed and we show examples of stable and unstable evolution, depending on the choice of parameters. We also discuss concrete choices of $\overrightarrow{V}$. We investigate $\overrightarrow{V}$ which were not, as far as we know, considered in this context, and which seem to be a very natural choice for the modelled phenomenon. We show that the pointwise assumption (7) is only relevant for special $\overrightarrow{V}$, which do not depend, or depend very weakly, on ρ. For $\overrightarrow{V}$ clearly dependent on ρ, the L^2-norm of the numerical solution ρ_h is decreasing only after an initial period of time. This does not contradict the scheme stability, but shows that a new analysis of these monotonicty and stability properties is needed.

The plan of this paper is as follows. Section 2 recalls the semi–implicit numerical scheme proposed in [5]. We discuss the choice of $\overrightarrow{V}$ and its computation in Sect. 3. We show in Sect. 4 the obtained simulations and discuss the choice of the time step for particular $\overrightarrow{V}$. We show the first confirmations of the so called Braess paradox. i.e. a heuristic observation that obstacles to the movement may facilitate it, and on the contrary, lack of obstacles may slow the movement down. We illustrate this Braess paradox for evacuation, leaving a more systematic study of the role of the obstacles for the future (see Sect. 5).

2 Numerical Scheme

In all what follows, we assume the geometry of Ω as in the Introduction and (3)–(4). We assume also that $\overrightarrow{V}$ may depend of x and ρ, we note $\overrightarrow{V} = \overrightarrow{V}(\rho)$.

Definition 1. *We say that $\rho : (0,T) \times \Omega \to \mathbb{R}$ solves the model (1), (5) (in the weak sense) if, for any $t \in (0,T)$, $\rho(t) \in H^1(\Omega)$, $\rho \geq 0$ and for any $\eta \in H^1(\Omega)$, any $t \in (0,T)$*

$$\int_\Omega \partial_t \rho(t)\, \eta + \int_\Gamma \rho(t)\, \eta\, \overrightarrow{V}(\rho(t)) \cdot \overrightarrow{\nu} - \int_\Omega \rho(t)\, \overrightarrow{V}(\rho(t)) \cdot \nabla \eta + \kappa \int_\Omega \nabla \rho(t) \cdot \nabla \eta \;=\; 0. \tag{8}$$

We have written $\int_\Omega f(t)$ for $\int_\Omega f(t,x)\, dx$.

One can verify by classical methods that under additional assumptions on $\overrightarrow{V}$, the solution ρ exists and, with the initial condition (6), is unique. We omit here the mathematical analysis of the model; of course many mathematical properties of ρ depend on the choice of $\overrightarrow{V}$ that we do not want to impose at this point. We state however an important monotonicty property and its relation to $\overrightarrow{V}$.

Definition 2. *The functions $m : \mathbb{R}_+ \to \mathbb{R}$ defined by*

$$m(t) = M(\rho(t)) = \int_\Omega \rho(t,x)\, dx. \tag{9}$$

shall be called the total mass function. *The function $s : \mathbb{R}_+ \to \mathbb{R}$ defined by*

$$s(t) = S(\rho(t)) = \int_\Omega \rho(t,x)^2\, dx \tag{10}$$

*shall be called the L^2–*stability function *for the equation (8) with $\rho(0) = \rho_0$.*

Lemma 1. *Let $\overrightarrow{V}$ satisfy (3)–(4). Let ρ be the solution to (1) with (5) and (6). The total mass function (9) is decreasing. The L^2–stability function (10) is decreasing in the neighborhood of t_0 if and only if t_0 is such that*

$$\int_\Omega \rho^2\, \mathrm{div}\, \overrightarrow{V} + 2\kappa \int_\Omega |\nabla \rho|^2 + \int_\Gamma \rho^2 \overrightarrow{V} \cdot \overrightarrow{\nu} \geq 0. \tag{11}$$

This condition is in particular fulfilled for $\overrightarrow{V}$ satisfying (7).

Proof. By posing $\eta = 1$, we obtain the first statement from (3)–(4). By posing $\eta = \rho$, again from (3)-(4) and the identity

$$2 \int_\Omega \rho\, \overrightarrow{V}(\rho) \cdot \nabla \rho \;=\; -\int_\Omega \rho^2\, \mathrm{div}\, \overrightarrow{V}(\rho) + \int_\Gamma \rho^2 \overrightarrow{V}(\rho) \cdot \overrightarrow{\nu}$$

we obtain:

$$\frac{1}{2} \frac{d}{dt} \int_\Omega \rho^2 \;=\; -\frac{1}{2} \int_\Omega \rho^2\, \mathrm{div}\, \overrightarrow{V}(\rho) \;-\; \kappa \int_\Omega |\nabla \rho|^2 \;+ \int_\Gamma \rho^2 \overrightarrow{V}(\rho) \cdot \overrightarrow{\nu}.$$

□

We define now the finite element spaces $V_h \subset H^1(\Omega)$, where h is, as usual, the mesh parameter, and look for the approximate solutions in V_h. Let $\Omega_h \subset \Omega$ be the triangulated, shape regular domain, with the mesh size parameter h. Let $(\cdot,\cdot)$ denote the L^2 product on Ω_h.

Definition 3 (cf. Def. 2 of [5]). *We define the sequence* $\{\rho_h^n\}_{n=0}^{\infty} \subset V_h$ *to be the* approximate FEM solution *of* (8) *if* ρ_h^n *satisfies the following* semi–implicit *first order scheme for any test function* $\eta_h \in V_h$*:*

$$\int_{\Omega_h} \left(\frac{\rho_h^{n+1} - \rho_h^n}{\Delta t} \right) \eta_h - \int_{\Omega_h} \rho_h^{n+1} \overrightarrow{V}(\rho^n) \cdot \nabla \eta_h + \kappa \int_{\Omega_h} \nabla \rho_h^{n+1} \cdot \nabla \eta_h + \\ + \int_{\Gamma_h} \rho_h^n \overrightarrow{V}(\rho^n) \cdot \overrightarrow{\nu}\, \eta_h = 0. \quad (12)$$

We say that the scheme is stable *from* n_0 *if for any* $n \geq n_0$*:*

$$(\rho_h^{n+1}, \rho_h^{n+1}) \leq (\rho_h^n, \rho_h^n).$$

Remark 1. The above definition is consistent with that of the semi–implicit scheme in [5, Def. 2], if we put

$$A_0(\varphi)(\rho,\eta) = -\int_{\Omega_h} \rho \overrightarrow{V}(\varphi) \cdot \nabla \eta + \kappa \int_{\Omega_h} \nabla \rho \cdot \nabla \eta, \quad (13)$$

$$B(\varphi)\rho = -\frac{1}{2} \rho \overrightarrow{V}(\varphi) \cdot \overrightarrow{\nu}, \quad (14)$$

and, for an arbitrary $\alpha > 0$,

$$A_1(\varphi)(\rho,\eta) = \frac{1}{2\alpha} \int_{\Gamma} \left[B(\varphi)\rho - \alpha\rho\right] \left[B(\varphi)\eta - \alpha\eta\right], \quad (15)$$

$$A_2(\varphi)(\rho,\eta) = \frac{1}{2\alpha} \int_{\Gamma} \left[B(\varphi)\rho + \alpha\rho\right] \left[B(\varphi)\eta + \alpha\eta\right]. \quad (16)$$

The notion of stability is also consistent with [5]. It is strong. A future study should include a weaker notion of stability, where the L^2 norm of the numerical solution is bounded.

Theorem 1. *[5]* **(CFL condition for stability).** *Let* $\alpha > 0$ *be an arbitrary constant and let's define* A_1 *as in* (14)–(15)*. The semi–implicit scheme* (12) *is stable under* (11) *and the abstract CFL condition*

$$\Delta t\, A_1(\rho_h)(u_h, u_h) \leq (u_h, u_h) \qquad \forall \rho_h, u_h \in V_h. \quad (17)$$

Proof. The proof is identical as in [5, Proof of Theorem 2], where the nonlinear case has already been considered. We have assumed there (7) to infer (11). □

In view of (14)–(15), we give below a more explicit form of the (CFL) condition.

Remark 2. If ρ solves the model (1), (5), the CFL condition (17) writes as

$$\frac{\Delta t \int_\Gamma u_h^2 \left(\overrightarrow{V}(\rho_h)\cdot\overrightarrow{\nu} - 2\alpha\right)^2}{8\alpha \int_{\Omega_h} u_h^2} \leq 1. \tag{18}$$

Note that κ does not appear in (18) explicitely. Instead, it has a crucial role in (11) in the case when $\operatorname{div}\overrightarrow{V}$, or $\int_\Omega \rho^2 \operatorname{div}\overrightarrow{V}(\rho)$, is not positive.

This form of CFL condition allows to find an optimal α. If we assume that $|\overrightarrow{V}|$ is bounded on Ω, we obtain $2\alpha_{opt} = \max_\Gamma |\overrightarrow{V}|$. With these assumptions, (18) is satisfied if

$$\frac{1}{4}\Delta t \left(2\max_\Gamma |\overrightarrow{V}| - \min_\Gamma |\overrightarrow{V}|\right) \frac{\int_\Gamma u_h^2}{\int_{\Omega_h} u_h^2} \;\leq\; C_0 \max_\Gamma |\overrightarrow{V}| \,\frac{\Delta t}{h} \;\leq\; 1. \tag{19}$$

Indeed, the last term on the lhs is of order oh $1/h$; it depends also on the mesh and on the degree of the elements. For a uniform mesh and P2 elements that we use in the sequel, $1/C_{0,u} = 6(1+\sqrt{2}) \approx 14.5$, see e.g. [11], where the authors propose to multiply $C_{0,u}$ by 10 so as to stay clearly away from the unstable region. In most simulations, we increase this constant even more. However, $\max|\overrightarrow{V}|$ may be difficult to estimate if it is not granted by construction.

3 Velocity

The velocity field $\overrightarrow{V}$ is a crucial element of the model. Apart from satisfying (3)–(4), it should reproduce the direction that the individual at x will follow so as to reach the exit. From the modelling point of view, V should be dependent on the space variable x, and on the density $\rho(x)$. From the analytical and numerical point of view, the important properties of $\overrightarrow{V}$ are (7) and (18).

A frequent simplification, that we also admit here, is to take

$$\overrightarrow{V} = \overrightarrow{V}\big(\rho(x)\big) = v\big(\rho(x)\big)\,\overrightarrow{W}(x), \tag{20}$$

where $\overrightarrow{W} : \Omega \to \mathbb{R}^2$ is a vector field giving the direction to follow at x, and $v : \mathbb{R} \to \mathbb{R}$ is a non-increasing function giving the scalar value of the velocity, responsible for a slow down when the density is bigger. So as to make v meaningful, $\overrightarrow{W}$ is often normalized: $|\overrightarrow{W}(x)| = 1$.

The most natural choice for $\overrightarrow{W}$ seems to be the vector field $-\nabla\Phi(x)$, where Φ is the distance to the exit. It is well known (see e.g. [2,4,13] and related works) that Φ is given by the so–called *eikonal equation*:

$$\Phi \in W^{1,p}(\Omega)\cap C(\bar{\Omega}) : \quad |\nabla\Phi(x)| = 1 \quad \text{for } x\in\Omega, \qquad \Phi(\xi) = 0 \quad \text{for } \xi\in\Gamma\,,$$

The eikonal equation is highly nonlinear. Many approximations of the distance function are used in applications (see [2]); a few however approximate its gradient. Among them, the most interesting one may be the solution of the p–Poisson problem. If

$$\Delta_p u = \operatorname{div}\left(|\nabla u|^{p-2}\,\nabla u\right),$$

we solve

$$\begin{cases} -\Delta_p \Psi_p(x) = 1 & \text{in } \Omega \\ \nabla \Psi_p \cdot \overrightarrow{\nu} = 0 & \text{on } \Gamma_w \\ \Psi_p = 0 & \text{on } \Gamma\,, \end{cases} \tag{21}$$

The result of [4] is that

$$\Psi_p \text{ converges to } \Phi \text{ strongly in } W^{1,m}(\Omega) \quad \text{as } p \to \infty, \qquad \text{for all } m \geq 1.$$

This means in particular that $|\nabla \Psi_p| \to 1$ as $p \to \infty$, a property which is very important. Thus, for bigger p, by taking $\overrightarrow{W} = -\nabla \Psi_p$, and $\overrightarrow{V}$ as in (20), we have a velocity field satisfying (3)–(4), $|\overrightarrow{W}| \approx 1$ and close to the vector field resulting from the eikonal equation. The CFL condition (19) is then also easier to satisfy and to check.

For $p = 2$, (21) is the linear Poisson equation. This case is of particular interest, because if we take $\overrightarrow{V} = -\nabla \Psi_2$ in (1), the condition (7) is satisfied directly. This $\overrightarrow{V}$, even if not a perfect choice from the modelling point of view, satisfies all our assumptions, and thus helps to determine constants in the CFL condition.

4 Simulations

4.1 Settings

In the simulations, we have considered a symmetric, nearly rectangular room of dimension 1×1.5, with two identical exits. We have placed obstacles in front of the exits, as in the figures below. The code has been coded and executed with the FreeFem++ software [6]. We used $P2$ elements. The mesh is shape regular, with h of order of 0.02. The maximal step size is $\Delta t = 0.01$. The initial density ρ_0 is constant. We have used the vector field (20) in two variants: with

$$\overrightarrow{W} = -\nabla \Psi_p$$

or

$$\overrightarrow{W}(x) = \frac{\Psi_p(x)}{|\Psi_p(x)|}, \tag{22}$$

where Ψ_p solves (21) for $p \in \{2, 3, 4, 5\}$ (we have also used rational values close to those). We shall clearly note in each experiment if $\overrightarrow{W}$ is normalized or not.

The p–Poisson equation (21) has been solved numerically by two methods:

1. the Newton method, see e.g. [12, Ch. 9],

2. the fixed–point (Picard) iterations: take u_0 solving $\Delta u_0 = -1$ and

$$\operatorname{div}\left(|\nabla u_{i-1}|^{p-2}\,\nabla u_{i-\frac{1}{2}}\right) = -1$$

for $i = 1, 2, \ldots$, with the boundary conditions as in (21). Additionally, we use a damping proposed in [1, (3.7), $\gamma = 0.5$], i.e. $u_i = \gamma u_{i-\frac{1}{2}} + (1-\gamma)u_{i-1}$. The equations were solved by FEM on the same grid.

The two approaches gave essentially the same results, the Newton method being, as expected, much faster. The unexpected behaviour was the nonconvergence of both methods for p bigger than 5. This value could be even slightly lower depending on the geometry and on the method, but we were unable to get it significantly higher, and this, apparently, independently of the mesh refinement. This effect was indeed reported in [1] as for the fixed–point method.

The scalar velocity function has a piecewise linear form:

$$v(\rho) = \min\left(v_{\max}, \max\left(1 - \frac{\rho}{\rho_{\max}}, 0\right)\right), \tag{23}$$

or a piecewise constant form:

$$v(\rho) = \frac{v_{\max}}{2} \quad \text{if } \rho \le \rho_{\max}; \qquad v(\rho) = 0 \quad \text{otherwise,} \tag{24}$$

or a constant form

$$v(\rho) = \frac{v_{\max}}{2}. \tag{25}$$

We take $v_{\max} = 1$ and $\rho_{\max} = 8$.

4.2 Linear Model, P = 2

At first, we perform our simulations with $p = 2$. Here, $\overrightarrow{W}$ is not normalized: $\overrightarrow{W} = -\nabla\Psi_2$ and v is constant as in (25). Thus, $\overrightarrow{V}$ satisfies the condition (7), and thus, the assumptions of 1.

We use five time steps Δt between 0.001 and 0.01 and draw in Fig. 1, the functions defined in Definition 2. (Note the log scale for t). The total mass function is decreasing only for $\Delta t \le 0.002$; the same is true for the stability function. It is clear, by Lemma 1, that these are the only cases where the scheme is stable.

4.3 $p \ge 2$

When $p > 2$, or if v is not constant, the property (7) is not satisfied anymore. In Fig. 2, we show experiments with $p \in \{2, 3, 5\}$. So as to minimize 'side effects', $\overrightarrow{W}$ is still not normalized: $\overrightarrow{W} = -\nabla\Psi_p$. The scalar velocity v is piecewise constant (24). As ρ does not exceed $\rho_{\max}$, our model is still in the linear regime, but (7) is not granted for $p > 2$.

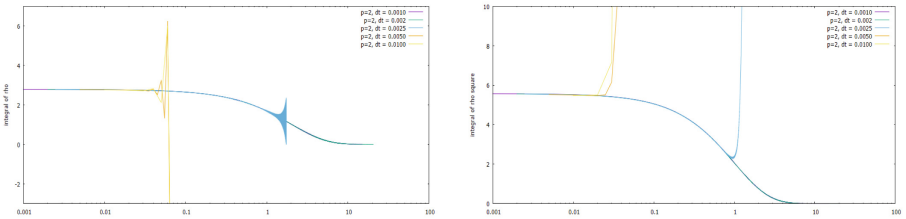

Fig. 1. Here, $\overrightarrow{V} = -0.5\nabla\Phi_2$. We compare the evolution for different time steps Δt. On the left, the total mass of pedestrians vs time. On the right, the stability function vs time. Both in log scale on the time axis. The decreasing curves correspond to $\Delta t = 0.002$ and $\Delta t = 0.001$, which fit almost perfectly. The light blue — to $\Delta t = 0.0025$, the others to bigger Δt. (Color figure online)

We take $\Delta t = 0.002$ for $p \in \{2, 3\}$ and $\Delta t = 0.01$ for bigger p, in view of the fact that $|\nabla \Psi_p|$ is considerably closer to 1 for these p. We observe on one hand, the stability of the scheme, and on the other, the effect of decreasing the total evacuation time with increasing p. In particular, for $p = 2$ the evacuation is very long. Finally, we verify that the Picard and Newton method applied to (21) give the same result. We have checked that with increasing p, the error between the two methods decreases.

4.4 Nonlinear Model, $p \geq 2$

We finally simulate the evacuation with a normed velocity field (22) and with v piecewise constant (24) and piecewise linear (23). Here, $\Delta t = 0.01$. The evolution is visualized in Fig. 3. Some violations of the non–negativity of ρ_h are observed when the model becomes nonlinear. The stability functions do not decrease in an initial period of time, after which they are all perfectly monotone, going down to zero. This means that (7) is no longer valid, and the weaker condition (11) becomes valid after this initial time. We postulate that our scheme is still stable, but within a larger definition of stability, meaning boundedness of the solution's L^2 norm. This approach should be considered in view of the properties of $\overrightarrow{V}$ itself.

We observe, as before, shortening of the evacuation time when p increases, but the influence of p is attenuated. Surpisingly enough, introducing a piecewise linear, decreasing velocity (23) does not shorten the evacuation time, and leads to bigger crowd densities. However, this comparison is still quite heuristic.

The Braess paradox clearly appears in Fig. 4: the upper part of the room, with more obstacles, evacuates more quickly and has less regions with high densities. This phenomenon can be observed for both forms of v, but a piecewise linear velocity (23) makes it clearer.

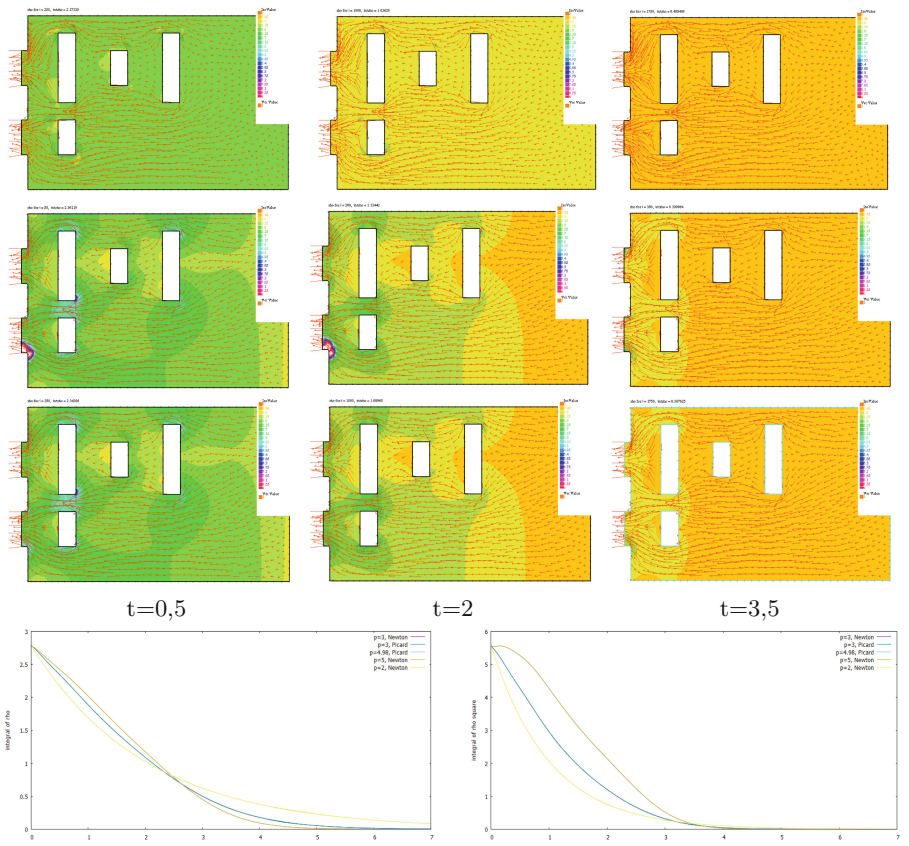

Fig. 2. The first three rows show the evolution of the crowd density with the velocity field $\overrightarrow{V} = v\nabla\Psi_p$ and p equal to, respectively, 2, 3, 5. We do not normalize the velocity field here. $\Delta t = 0.002$ when p equals 2 or 3, $\Delta t = 0.01$ for $p = 5$. In the fourth row, on the left, the evolution of the total mass of pedestrians: in yellow for $p = 2$, in blue/green for $p = 3$, in brown $p = 5$ (4.98 for the Picard method). On the right, the stability function for each case. (Color figure online)

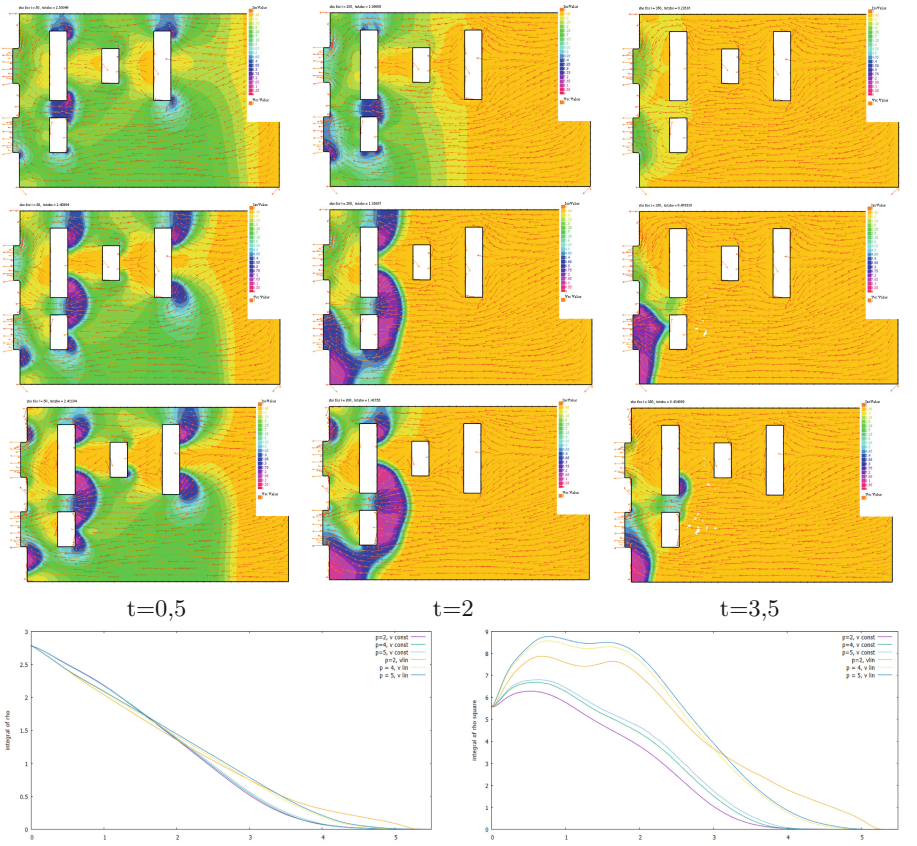

Fig. 3. Evolution with a velocity field $\overrightarrow{V} = v\overrightarrow{W}$ where $\overrightarrow{W}$ is normed according to (22). $\Delta t = 0.01$. First row, the scalar function v is piecewise constant (24) and $p = 2$. Second row, the scalar function v is piecewise linear (23) and $p = 2$. Third row, the scalar function v is piecewise linear (23) and $p = 4$. Below, on the left, the evolution of the total mass of pedestrians, with v piecewise constant and p taking the values 2, 5 (steeper functions) and v piecewise linear and p taking the values 2, 4, 5. On the right, the stability function for each case. Here, the influence of p on the dynamics is smaller than in the previous case.

5 Conclusions

We have concentrated here on the role of the velocity field $\overrightarrow{V}$ for the evacuation dynamics, in particular when the direction of $\overrightarrow{V}$ is given by the p–Poisson equation (21). We have shown that bigger p shorten the evacuation time. We have also seen the Braess paradox appearing in evacuation.

In this context, a more systematic study of the role of 1) the dependence of the velocity field on ρ 2) the parameter κ (which may also be dependent on ρ), and finally 3) the geometry, is to be performed. At this end, we need a

mathematical study of a weaker condition for stability: $(\rho_h^n, \rho_h^n) \leq C$. We also hope to find a numerical method for solving the p–Poisson equation for larger p.

References

1. Bakker, J.C.: Wall-distance calculation for turbulence modelling. Bachelor Thesis, Delft University of Technology (2018)
2. Belyaev, A., Fayolle, P.-A.: On variational and PDE-based distance function approximations. Compu.r Graphics Forum **34**(8), 104–118 (2015)
3. Colombo, R.M., Gokieli, M., Rosini, M.D.: Modeling crowd dynamics through hyperbolic - elliptic equations. In: Non-Linear Partial Differential Equations, Mathematical Physics, and Stochastic Analysis – The Helge Holden Anniversary Volume, pp. 111–128. EMS Series of Congress Reports, May 2018
4. Bhattacharya, T., DiBenedetto, E., Manfredi, J.: Limits as $p \to \infty$ of $\Delta_p u_p = f$ and related extremal problems. Rend. Sem. Mat. Univ. Politec. Torino **47**, 15–68 (1989)
5. Gokieli, M., Szczepańczyk, A.: A numerical scheme for evacuation dynamics. In: Wyrzykowski, R., Deelman, E., Dongarra, J., Karczewski, K. (eds.) PPAM 2019. LNCS, vol. 12044, pp. 277–286. Springer, Cham (2020). https://doi.org/10.1007/978-3-030-43222-5_24
6. Hecht, F.: New development in FreeFem++. J. Numer. Math. **20**(3–4), 251–265 (2012)
7. Hughes, R.L.: A continuum theory for the flow of pedestrians. Transp. Res. Part B Methodol. **36**(6), 507–535 (2002)
8. Hughes, R.L.: The flow of human crowds. Annu. Rev. Fluid Mech. **35**(1), 169–182 (2003)
9. Jiang, Y., Zhou, S., Tian, F.-B.: Macroscopic pedestrian flow model with degrading spatial information. J. Comp. Sci. **10**, 36–44 (2015)
10. Kachroo, P.: Pedestrian Dynamics: Mathematical Theory and Evacuation Control. CRC Press (2009)
11. Kamga, J.-B.A., Després, B.: CFL condition and boundary conditions for DGM approximation of convection-diffusion. SIAM J. Numer. Anal. **44**(6), 2245–2269 (2006)
12. M. G. Larson and F. Bengzon. The finite element method: theory, implementation, and practice. Texts in Computational Science and Engineering 10, 2010
13. Twarogowska, M., Goatin, P., Duvigneau, R.: Macroscopic modeling and simulations of room evacuation. Appl. Math. Model. **38**(24), 5781–5795 (2014)